Journal of Molecular Liquids 446 (2026) 129306

Contents lists available at ScienceDirect

Journal of Molecular Liquids

journal homepage: www.elsevier.com/locate/molliq

Investigating the bimodality of liquid water via chemical bond descriptors and k-means clustering analysis

Mateus Quintano[a,*], Ayesh Madushanka[b], Carlos V. Santos-Jr[c], Francielle C. Machado[a], Elfi Kraka[b], Ricardo L. Longo[a], Renaldo T. Moura Jr.[b,d,**]

[a] Department of Fundamental Chemistry, Federal University of Pernambuco Recife, PE 50740-560, Brazil
[b] Computational and Theoretical Chemistry Group (CATCO) Department of Chemistry, Southern Methodist University Dallas, TX 75275, USA
[c] Department of Chemistry, Federal University of Paraíba João Pessoa, PB 58033-455, Brazil
[d] Academic Unit of Cabo de Santo Agostinho, Federal Rural University of Pernambuco, Cabo de Santo Agostinho, PE 54518-430, Brazil

HIGHLIGHTS

- Local bond descriptors reveal bimodality in liquid water's hydrogen bonds.
- HDL and LDL show distinct, wide-ranging distributions of hydrogen-bond properties.
- K-means clustering distinguishes LDL and HDL hydrogen-bonding regimes.

GRAPHICAL ABSTRACT

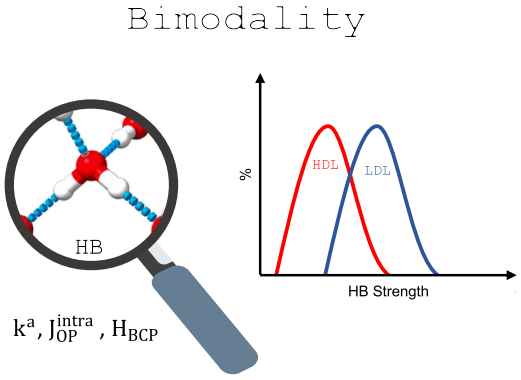

ARTICLE INFO

Keywords:
Chemical bond descriptors
Liquid water
Bimodal behavior
Infrared spectra

ABSTRACT

Liquid water exhibits anomalous behavior, with several of its physical and chemical properties deviating from those of ordinary liquids. Some of these anomalies stem from a bimodality observed in macroscopic properties such as density, isothermal compressibility, and specific heat, as well as the radial distribution function and vibrational spectra, which reflect the collective structural dynamics of liquid water. The infrared spectrum is particularly sensitive to hydrogen-bonded arrangements, thus it could be a crucial link between macroscopic properties and microscopic interactions. This study utilizes structural models that align with the experimental infrared spectrum of liquid water, offering a novel proof of concept. It bridges a critical gap by demonstrating how the bimodality of liquid water can be revealed through fully localized chemical bond descriptors. These descriptors are derived from local vibrational mode theory, the chemical bond overlap model and its topological extension, as well as the quantum theory of atoms in molecules. Key findings reveal that the local force constant, intra-overlap Coulomb repulsion, and Cremer and Kraka's energy density associated with hydrogen bonds exhibit bimodal behavior. Notably, by employing the unsupervised machine learning algorithm K-means for clustering analysis, we identified distinct regimes of hydrogen-bond strength, revealing systematic patterns that differentiate

* Corresponding author.
** Corresponding author at: Academic Unit of Cabo de Santo Agostinho, Federal Rural University of Pernambuco, Cabo de Santo Agostinho, PE 54518-430, Brazil.
Email addresses: mateusmquintano@gmail.com (M. Quintano), renaldo.tmoura@ufrpe.br (R.T. Moura Jr.).

https://doi.org/10.1016/j.molliq.2026.129306
Received 21 December 2025; Received in revised form 19 January 2026; Accepted 20 January 2026
Available online 21 January 2026

the low-density liquid and high-density liquid networks. Overall, this study reinforces the concept that liquid water consists of two distinct types of local structures, providing new insights into its bimodal nature and advances in this field.

1. Introduction

The unique properties of liquid water have profoundly influenced the evolution of life on Earth [1]. Liquid water exhibits anomalies that are evident even under ambient conditions, as reflected in various physical and chemical properties, such as density, isothermal compressibility, and heat capacity [2–4]. In this context, the temperature-dependent bimodal behavior of liquid water refers to changes in the slope of a given property with temperature. This anomalous behavior seems to arise from the coexistence of two distinct phases, characterized by competition between two local structures. A liquid-liquid transition between high-density liquid (HDL) and low-density liquid (LDL) in supercooled water was initially proposed [5,6] and later experimentally confirmed using X-ray pulses [7]. The presence of these two local structures can be strongly inferred even under moderate conditions [8–12]. Notably, the infrared spectrum of liquid water, which reflects hydrogen-bonded arrangements and arises from collective structural features, similar to the radial distribution function, also exhibits bimodality. This spectrum can be described as a temperature-dependent linear combination of two temperature-independent spectra [12].

Ultimately, HDL and LDL differ in their topologies [11,13–16], with LDL exhibiting a higher degree of structural order, which promotes the formation of hydrogen bonds [17]. Existing research recognizes LDL and HDL in liquid water as part of a continuous distribution of hydrogen bonds, where each local structure corresponds to a broad and diverse range of hydrogen-bonding interactions [12]. While theoretical studies have explored structural models based on chains and dodecahedra [17], which generate two infrared spectra closely matching the experimentally measured temperature-independent ones, thereby supporting bimodal behavior [12], a systematic chemical bond descriptor approach to this continuous hydrogen-bonding distribution remains absent. Surprisingly, the intrinsic bond strength and nature of these noncovalent interactions in the proposed local structures have yet to be thoroughly investigated.

To that end, this study introduces a new approach for investigating the anomalous behavior of liquid water, focusing on the structural models [17] that capture the bimodality of its infrared spectrum [12], that is, chains for HDL and dodecahedra for LDL (see Fig. 1). Given the high configurational variability of hydrogen-bonded networks, it might be unlikely for these structural models to directly correspond to molecular dynamics results [17]. However, it is likely that they might correspond to average or equilibrium structural models because they provide infrared spectra that agree remarkably well with experiments [12]. Our goal was to characterize the proposed LDL and HDL structures using local vibrational mode (LVM) theory, addressing the need for a local vibrational spectroscopy approach to probe liquid water, as emphasized in the literature [18,19]. For the first time, we combined LVM with the chemical bond overlap model and its topological extension (OP/TOP) [20–22], the quantum theory of atoms in molecules (QTAIM) [23,24], and natural bond orbital (NBO) analysis [25,26] to achieve a more holistic understanding of hydrogen bonding in liquid water. Of particular importance to this analysis is the use of K-means clustering [27,28], an unsupervised machine learning approach, to investigate how hydrogen-bond strength organizes into distinct regimes that may differentiate low- and high-density liquid structures.

2. Computational methods

There is a trade-off between the number of water molecules forming a molecular cluster that exhibits a vibrational spectrum similar to that of liquid water and the model employed [29,30]. Small water clusters up to hexamers have limitations in accurately capturing the vibrational spectrum of liquid water [29]. Among various models proposed to explain the properties and anomalies of water [2], the clathrate model stands out, with pentagonal dodecahedra emerging as a key polyhedral component in the liquid water structure envisioned by Pauling [31]. In this study, we adopted structural models from the literature [17], which are based on clathrate-like fused dodecahedra (103 molecules) composed solely of pentagons to represent LDL and chain-like structures (72 molecules) to represent HDL (see Fig. 1). These models were used to compute infrared spectra, yielding results consistent with the experimentally observed bimodality in previously reported temperature-independent spectra [12].

All electronic structure calculations were performed using the Gaussian 16 software [32] at the density functional theory (DFT) level [33]. The equilibrium geometries of the structures, with initial Cartesian coordinates sourced from the literature [17], along with their corresponding Hessian matrices and normal vibrational modes, were computed using the ωB97X-D functional [34] and the polarizable continuum model (PCM) [35] with water as the solvent, which provides an economical description of vibrational spectroscopy in solution [36], in

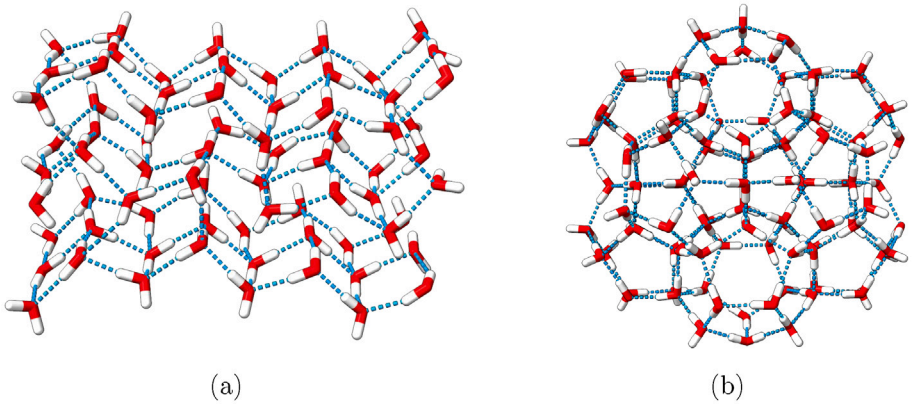

Fig. 1. Optimized geometries from this work at the ωB97X-D(PCM)/6-311G* level of theory, based on the structural models of chains for HDL (a) and dodecahedra for LDL (b) [17], visualized using UCSF ChimeraX [38].

combination with the cost-effective 6-311G* basis set [37]. The computed infrared spectra data were prepared using UCSF ChimeraX [38], while the elegant visualizations in the following sections were created with Seaborn [39]. The Cartesian coordinates of the optimized geometries are available in the Supplementary Material for reference. With the electronic structure results in hand, the methods described below were employed to obtain the chemical bond descriptors.

To characterize hydrogen bonding and structural bimodality in liquid water, we employ complementary quantum-chemical analysis methods that probe different but interconnected aspects of chemical bonding. The LVM theory links vibrational spectroscopy to intrinsic bond strength by transforming delocalized normal modes into bond-specific local modes. The OP/TOP offers a measure of bond strength rooted in constructive orbital interactions, quantifying electron sharing between atoms through overlap densities while excluding nodal and destructive-interference contributions. QTAIM provides a topological description based on the energy density at bond critical points, enabling assessment of the covalent versus electrostatic character of hydrogen bonds. The NBO analysis complements this picture by identifying donor–acceptor interactions and charge-transfer effects underlying hydrogen bonding. Finally, clustering analysis is used as a statistical tool to correlate and classify selected bond descriptors, allowing objective identification of distinct hydrogen-bond populations associated with LDL and HDL structures.

2.1. Local vibrational mode theory

Normal coordinates arise as linear combinations of internal coordinates within the GF formalism [40]. As a result, normal vibrational modes are typically delocalized across the molecule, which limits the usefulness of the associated normal mode frequencies and force constants as direct indicators of bond strength. This delocalization issue is addressed by LVM [41,42], originally introduced by Konkoli and Cremer [43]. The core principle of LVM is to extract local vibrational modes from delocalized normal vibrational modes, as these capture intrinsic bond properties. The subtleties of local mode analysis have been recently discussed in several reviews [41,42,44]. Therefore, only a few key aspects of the method are described below.

The normal vibrational modes in internal coordinates, $\mathbf{d}_n$ ($n = 1, \ldots, 3N - \Sigma$; for molecules with N atoms, $\Sigma = 5$ for linear molecules and $\Sigma = 6$ otherwise), along with the diagonal force constant matrix, $\mathbf{K}$, can be used to determine the local mode vectors, $\mathbf{a}_n$, associated with the internal coordinates, q_n, as derived by Konkoli and Cremer [43]:

$$\mathbf{a}_n = \frac{\mathbf{K}^{-1}\mathbf{d}_n^{\dagger}}{\mathbf{d}_n\mathbf{K}^{-1}\mathbf{d}_n^{\dagger}} . \tag{1}$$

Note that $\mathbf{d}_n$ and $\mathbf{K}$ are readily accessible from standard quantum chemistry software following vibrational frequency analysis.

The calculation of the local force constant, k_n^a, is performed as:

$$k_n^a = \mathbf{a}_n^{\dagger}\mathbf{K}\mathbf{a}_n = \left(\mathbf{d}_n\mathbf{K}^{-1}\mathbf{d}_n^{\dagger}\right)^{-1} . \tag{2}$$

For a comprehensive compilation of examples, refer to Refs. [41,42] and the references therein. More recent applications of k_n^a as a robust bond strength descriptor, encompassing both covalent and non-covalent interactions can be found e.g., in Refs. [45–55]. Investigations on hydrogen bonding in the water dimer, in solvated Ca and Mg ion clusters and in ice can be found in Refs. [56–59], respectively. In the context of the LModeAGen protocol [60], the local mode analysis was performed in this work with the standalone LModeA package [61].

2.2. Chemical bond overlap model and the OP/TOP extension

The intricacies of OP/TOP have been thoroughly documented in the literature over the years [20–22]. Therefore, the subsequent description focuses on highlighting a few essential elements of the method.

Constructive or destructive interference arises from the combination of typically orthogonal atomic orbitals to form molecular orbitals, which affects the spatial electron density distribution. In addition, nodes are a result of the cancellation of contributions from different atomic orbitals by interference. To circumvent nodal and negative regions, the overlap density, $\rho_{\mathrm{OP}}(\vec{r})$, is computed by numerically evaluating two-center terms of each molecular orbital on discrete grid points, $\vec{r}$. This method isolates positive (constructive) contributions, as detailed in a recent study [21]. The expression for $\rho_{\mathrm{OP}}(\vec{r})$ is:

$$\rho_{\mathrm{OP}}(\vec{r}) = 2\sum_{l}^{M} n_l \sum_{i\in A}^{m}\sum_{j\in B}^{m} c_{li}c_{lj}\phi_i(\vec{r})\phi_j(\vec{r}) \tag{3}$$

where $\vec{r} \in \{\vec{r} \mid \rho_{\mathrm{OP}}(\vec{r}) > 0\}$,

in which l spans all M molecular orbitals (the spatial components of spin-orbitals), with n_l denoting their occupancies. The parameter m represents the total number of atomic orbitals (AOs), while c_{li} are the coefficients of the linear combination of atomic orbitals (LCAO) expansion, and ϕ_i denotes the primitive or contracted functions defining the AOs. The overlap (OP) density, $\rho_{\mathrm{OP}}(\vec{r})$, quantifies the two-center contribution to the total electron density, capturing electron sharing between atoms. The integrated overlap density, ρ_{OP}, obtained by integrating Eq. (3) over all space [62], represents the electron density shared within a bond.

The intra-overlap Coulomb repulsion, J, in the OP/TOP framework, is given by:

$$J_{\mathrm{OP}}^{\mathrm{intra}} = \int \rho_{\mathrm{OP}}\left(\mathbf{r}_1\right) r_{12}^{-1} \rho_{\mathrm{OP}}\left(\mathbf{r}_2\right) \mathrm{d}\mathbf{r}_1 \mathrm{d}\mathbf{r}_2 , \tag{4}$$

with r_{12} denoting the distance between points $\mathbf{r}_1$ and $\mathbf{r}_2$, where the overlap densities $\rho_{\mathrm{OP}}(\mathbf{r}_1)$ and $\rho_{\mathrm{OP}}(\mathbf{r}_2)$ are evaluated. In general, ρ_{OP} is higher in electron-rich bonds. Notably, bonds with localized regions of concentrated OP density often exhibit increased values of $J_{\mathrm{OP}}^{\mathrm{intra}}$, positioning it as a descriptor of bond strength as well. The OP/TOP analysis was performed utilizing the ChemBOS software [63]. The Supplementary Material provides a visualization of the bond overlap density maps, clearly emphasizing the distinct overlap density patterns between chains and dodecahedra.

2.3. Quantum theory of atoms in molecules

By employing Bader's quantum theory of atoms in molecules (QTAIM) [23,24], the local force constant information was supplemented with Cremer and Kraka's energy density at the bond critical point (BCP) of the electron density, $H(\mathbf{r}_b)$. In other words, the Cremer-Kraka criterion [64,65] was employed to evaluate the covalent character of hydrogen bonds, based on the energy density, $H(\mathbf{r})$, defined as:

$$H(\mathbf{r}) = G(\mathbf{r}) + V(\mathbf{r}) \tag{5}$$

where $G(\mathbf{r})$ represents the Lagrangian form of the kinetic energy density (positive, destabilizing), and $V(\mathbf{r})$ corresponds to the potential energy density (negative, stabilizing). $H(\mathbf{r})$ is equivalent to $-K(\mathbf{r})$, i.e., the negative of the Hamiltonian form of the kinetic energy density [66]. If $H(\mathbf{r}_b)$ is negative, the bond or interaction is predominantly covalent. Conversely, if it is positive, the bond or interaction is primarily electrostatic [64,65]. For convenience, $H(\mathbf{r}_b)$ is denoted as H_{BCP} throughout the text. The QTAIM analysis was conducted using the AIMAll software package [66].

2.4. Natural bond orbital analysis

According to the natural bond orbital (NBO) analysis, hydrogen bond formation involves two competing effects: hyperconjugation, which weakens and elongates the proton-donating bond, and rehybridization, which strengthens and shortens it [67]. The orbital interaction between the antibonding orbital, σ^*, of the hydrogen bond donor and the lone pair orbital, n, of the acceptor can be examined through orbital occupancies, which serve as indicators of these interactions. These occupancies were determined using NBO analysis [25,26], as implemented in the NBO 6 program [68].

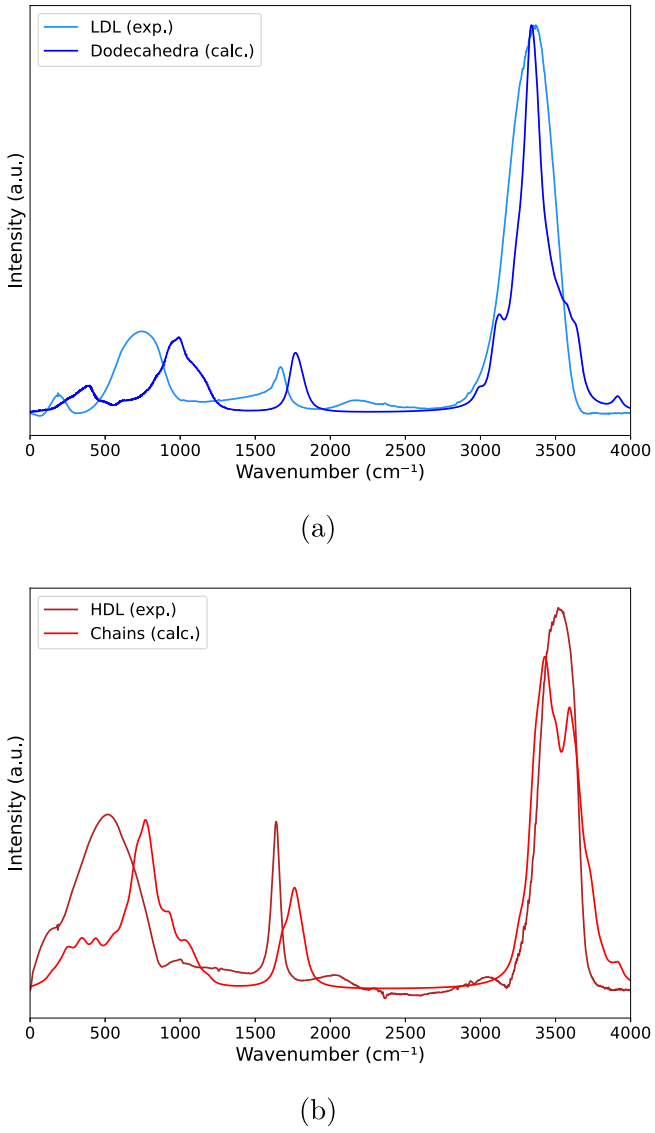

Fig. 2. Infrared spectra calculated (calc.) at the ωB97X-D(PCM)/6-311G* level of theory, using initial geometries from the literature for the structural models [17], alongside experimental (exp.) spectra [12]: (a) comparison of LDL (exp.) with dodecahedra (calc.); (b) comparison of HDL (exp.) with chains (calc.).

2.5. Clustering analysis

To uncover patterns and correlations in intrinsic bond strength, represented by the local force constant (k^a), with the bond length (r), thereby enabling comparison with the literature on water ices [59], as well as with Cremer and Kraka's energy density (H_{BCP}) to probe covalency [64,65], K-means clustering [27,28] was employed. The optimal number of clusters was objectively determined using the Elbow [69,70] and Silhouette methods [71], which evaluate cluster compactness and separation, respectively.

3. Results and discussion

Fig. 2 validates the structural models predicted based on the infrared spectrum of liquid water in the full range of 0−4000 cm^{-1} [17]. In the OH-stretch region, the structural models are consistent with the experimentally derived spectra. The torsional and bending modes show frequency discrepancies, which are expected given the harmonic approximation underlying the computed spectra, as discussed in detail in the literature by the proponents of the structural models adopted herein [17]. For comparisons, each spectrum (calculated and experimental) was normalized to the maximum intensity of the reference HDL or LDL

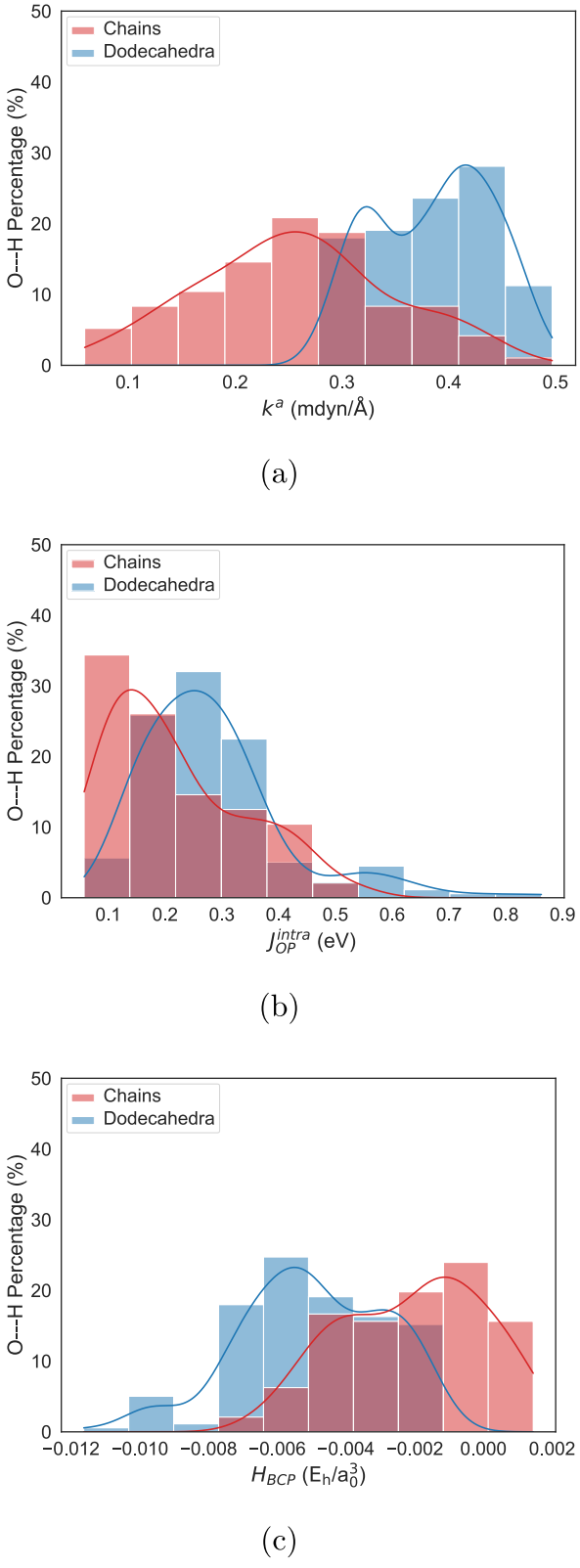

Fig. 3. Bimodality in the hydrogen bond distribution in chains and dodecahedra, as revealed by the chemical bond descriptors: (a) local force constant, k^a, (b) intra-overlap Coulomb repulsion, $J_{\mathrm{OP}}^{\mathrm{intra}}$, and (c) Cremer and Kraka's energy density, H_{BCP}.

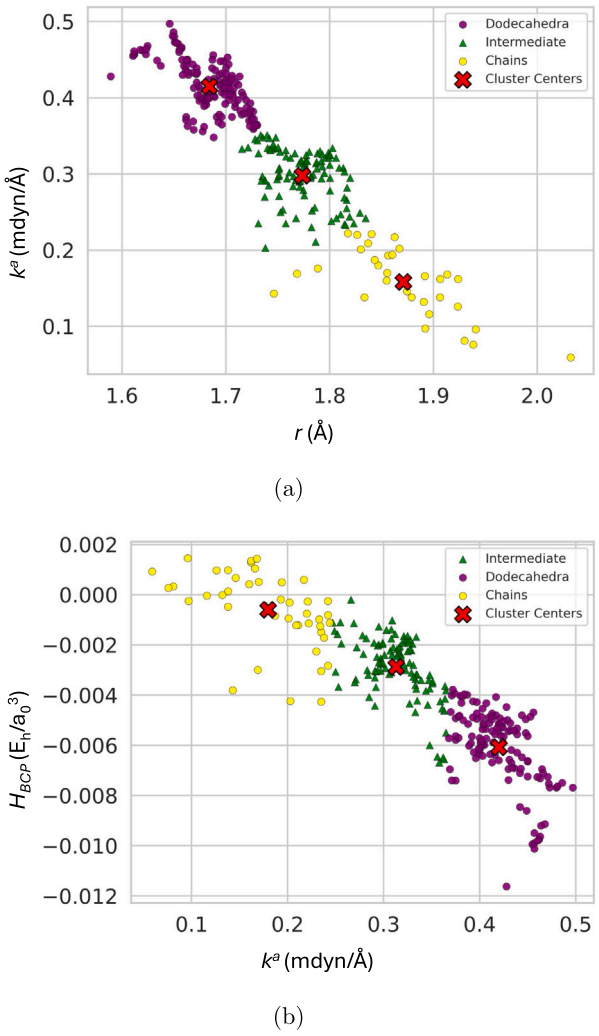

Fig. 4. K-means clustering analysis for chains and dodecahedra hydrogen bond relationships between the chemical bond descriptors: (a) local force constant (k^a) versus bond length (r), a Badger-type relationship, and (b) Cremer and Kraka's energy density (H_{BCP}) versus local force constant (k^a).

spectrum, separately in the theoretical and experimental data. The close agreement between the calculated and the experimental infrared spectra is the main justification for the choice of the theoretical level and the models for HDL and LDL (Fig. 1). It is expected that this approach will provide an adequate description of the electronic structure of HDL and LDL, with reliable local properties.

Although liquid water can be probed by infrared spectroscopy, the conventional approach correlating the hydrogen bond stretching normal frequency with the corresponding bond length has been reported to suffer from ambiguity [72,73]. Hence, a local approach, focusing on the local O–H and O···H vibrations in liquid water, is highly relevant for refining the interpretation of intrinsic spectral signatures behind the vibrational spectrum [18,19]. With that goal in mind, the scope of the present discussion is not normal mode analysis, but rather chemical bond descriptors of a local nature. A comprehensive spectral analysis based on normal mode analysis can be found elsewhere [17].

Of interest here is the bimodality of liquid water revealed by the chemical bond descriptors, k^a, $J_{\mathrm{OP}}^{\mathrm{intra}}$, and H_{BCP} for hydrogen bonds, as shown in Fig. 3. An equivalent analysis for covalent O–H bonds is provided in the Supplementary Material, revealing that bimodality in this context occurs exclusively in hydrogen bonds. Fig. 3 further supports the proposal that each local structure corresponds to a broad and extensive range of hydrogen bonds [12] within a continuous distribution, regarding local force constant, intra-overlap Coulomb repulsion, and energy density. Overall, with respect to k^a, $J_{\mathrm{OP}}^{\mathrm{intra}}$, and H_{BCP}, the hydrogen bonds in dodecahedra exhibit higher intrinsic bond strength, more pronounced electron-rich features, and a higher degree of covalency, respectively. This finding is reassuring because LDL prevails at low temperatures with stronger hydrogen bonds, while HDL becomes dominant at high temperatures, forming weaker hydrogen bonds [12].

The unsupervised machine learning K-means clustering approach, as shown in Fig. 4, enabled the identification of distinct structural and energetic regimes within the dataset [74], thereby providing deeper insight into the underlying physicochemical relationships governing hydrogen bond strength between chains and dodecahedra. It is noteworthy that the local force constant allows for the generalization of Badger's rule, establishing a universal relationship between bond length and the corresponding local force constant, provided that all considered bonds exhibit similar electronic features [75]. Fig. 4(a) indicates that the hydrogen bonds in chains and dodecahedra follow the generalized Badger's rule: the shorter the interatomic distance, the stronger the interaction. Accordingly, Fig. 4(b) aligns with the trend that weaker hydrogen bonds exhibit greater electrostatic character [46,76].

In the Elbow method, the optimal number of clusters is typically determined at the point where the rate of decrease in the within-cluster sum of squares (WCSS) significantly diminishes, indicating the onset of slope flattening. This 'elbow' point represents the best trade-off between model simplicity and performance [77]. Conversely, the Silhouette method identifies the optimal number of clusters by selecting the configuration that yields the highest average silhouette score, signifying that the clusters are distinct, dense, and well-separated [78]. For both of our k^a relationships, the results from both the Elbow and Silhouette analyses consistently indicated that 3 is the optimal number of clusters. The Elbow graphs and Silhouette scores are provided in the Supplementary Material.

In the relationship between k^a and r (Fig. 4a), the yellow cluster is exclusively derived from chains up to a k^a value of approximately 0.25 mdyn/Å. A transition between chains and dodecahedra is observed within the intermediate green cluster. Finally, the purple cluster primarily consists of dodecahedra hydrogen bonds, with only a marginal chains contribution observed, and becomes purely dodecahedra-derived above the k^a value of 0.4 mdyn/Å. High k^a values have been previously shown to indicate stronger and more linear hydrogen bonds [47].

Alternatively, the relationship between k^a and the Cremer and Kraka's energy density H_{BCP} (Fig. 4b) reveals a similar clustering pattern to the k^a vs. r analysis. The yellow cluster exhibits a more electrostatic character, while the purple cluster demonstrates a stronger covalent-like hydrogen bond character. The green cluster represents the transition between these two extremes.

Madushanka et al. [47] investigated approximately 2200 hydrogen bonds in a wide range of systems and established a clear correlation between the hydrogen-bond angle and k^a. Their analysis revealed that hydrogen bonds with larger values of k^a are predominantly linear, whereas those with lower k^a values exhibit increased nonlinearity. These findings, together with the results presented in this work, suggest that hydrogen bonds with lower k^a correspond to weaker interactions and more disordered structural arrangements (increasing nonlinearity), analogous to HDL [79,80], while those with higher k^a values are associated with stronger, more linear interactions characteristic of more ordered structural arrangements, analogous to LDL [81]. This behavior is consistent with the hydrogen-bond dynamics reported by Nanayakkara et al. [59] for ice. Furthermore, according to the literature [82–84], the structural transition from LDL to HDL involves the breaking and reforming of the hydrogen bonds, leading to faster orientational dynamics and increasing structural disorder; consequently, HDL is characterized by more distorted hydrogen bonds with shorter lifetimes, whereas LDL maintains longer-lived, more linear ones.

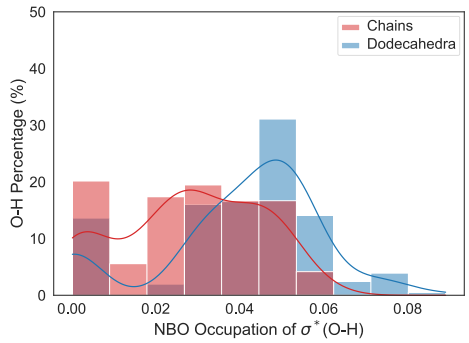

Fig. 5. NBO occupancies associated with O–H···O interactions in both chains and dodecahedra.

Finally, the results of the NBO analysis focusing on the orbital occupancies associated with O–H···O interactions in both chains and dodecahedra are shown in Fig. 5. In the occupation ranges of 0.00–0.03 and 0.05–0.09, the hydrogen bond distributions appear consistent with the literature, supporting the expectation that LDL and HDL exhibit similar behaviors regarding their hydrogen-bond acceptor characteristics [12]. An increase in the population of the σ^* orbital indicates a direct overlap with the n orbital, enhancing the hyperconjugative $n \rightarrow \sigma^*$ electron transfer [67]. As shown in Fig. 5, dodecahedral structures exhibit a higher fraction at elevated σ^* populations, consistent with the trend observed in Fig. 4.

Together, these findings demonstrate that the localized chemical bond descriptors applied in this work provide a distinctive and relevant framework for understanding the bimodality of liquid water, enriching current perspectives on this phenomenon.

4. Conclusion

The present work provides the first comprehensive assessment of hydrogen bonding in the two proposed local structures of liquid water within the structural models based on its infrared spectrum, applying a combination of LVM, OP/TOP, QTAIM, and NBO chemical bond descriptors and the unsupervised machine learning algorithm K-means clustering [27,28]. The adopted structural models [17] provide infrared spectra that match experiments remarkably well [12]. A possible critique of these structural models might be their difficulty in expressing a direct outcome of molecular dynamics [17]. However, given the agreement with the experimental spectra, these structural models might be considered as an average outcome of liquid simulation results.

The most significant finding of our study is the identification of distinct structural and energetic regimes within our dataset, revealing deeper physicochemical relationships underlying hydrogen-bond strength in liquid water. In particular, the use of K-means clustering demonstrates how hydrogen-bond strength naturally organizes into distinct regimes that may differentiate low- and high-density liquid structures within the structural models, chains for HDL and dodecahedra for LDL [17], as supported by experimental infrared spectra of liquid water [12]. Overall, our results strengthen the proposal that liquid water consists of two distinct local structures, contributing to the growing evidence of its bimodal nature.

CRediT authorship contribution statement

Mateus Quintano: Writing – review & editing, Writing – original draft, Visualization, Validation, Software, Project administration, Methodology, Investigation, Formal analysis, Data curation, Conceptualization. **Ayesh Madushanka:** Writing – review & editing, Validation, Software, Methodology, Investigation, Formal analysis, Data curation, Conceptualization. **Carlos V. Santos-Jr:** Visualization, Validation, Software, Methodology, Formal analysis, Data curation. **Francielle C. Machado:** Visualization, Software, Methodology, Investigation, Formal analysis, Conceptualization. **Elfi Kraka:** Writing – review & editing, Software, Resources, Formal analysis, Conceptualization. **Ricardo L. Longo:** Writing – review & editing, Validation, Supervision, Software, Resources, Project administration, Methodology, Investigation, Funding acquisition, Formal analysis, Conceptualization. **Renaldo T. Moura Jr.:** Writing – review & editing, Supervision, Software, Resources, Project administration, Methodology, Investigation, Formal analysis, Conceptualization.

Declaration of competing interest

The authors declare that they have no known competing financial interests or personal relationships that could have appeared to influence the work reported in this paper.

Acknowledgements

The authors thank Southern Methodist University's O'Donnell Data Science and Research Computing Institute for providing generous computational resources. MQ thanks Fundação de Amparo a Ciência e Tecnologia do Estado de Pernambuco (FACEPE) for Postdoctoral Fellowship No. BFP-0039-1.06/24, as well as Dr. Kraka and Southern Methodist University for the ColdFront HPC membership. FCM thanks FACEPE for Doctorate Scholarship No. IBPG-1927-1.06/24. RTMJr thanks the Brazilian National Council for Scientific and Technological Development (CNPq), Grant Nos. 406483/2023-0, 310988/2023-3, and 404742/2024-6. RLL thanks CNPq for the PQ-fellowship (Proc. 308000/2022-6).

Appendix A. Supplementary material

Supplementary material associated with this article is available online.

- SM-bimodality-paper.pdf: Distribution analyses of chemical bond descriptors for O–H bonds, Elbow and Silhouette analyses, bond overlap density maps for the local structures, and the Cartesian coordinates of the optimized geometries are provided.

Supplementary data for this article can be found online at doi:10.1016/j.molliq.2026.129306.

Data availability

Data will be made available on request.

References

[1] M. Chaplin, Water structure and science, 2022. https://water.lsbu.ac.uk/water/index.html.
[2] R. Ludwig, Water: from clusters to the bulk, angew, Chem. Int. Ed. 40 (2001) 1808–1827, https://doi.org/10.1002/1521-3773(20010518)40:10<1808::AID-ANIE1808>3.0.CO;2-1
[3] A. Nilsson, L.G.M. Pettersson, The structural origin of anomalous properties of liquid water, NAT, Commun. 6 (2015) 8998, https://doi.org/10.1038/ncomms9998
[4] P. Gallo, K. Amann-Winkel, C.A. Angell, M.A. Anisimov, F. Caupin, C. Chakravarty, E. Lascaris, T. Loerting, A.Z. Panagiotopoulos, J. Russo, J.A. Sellberg, H.E. Stanley, H. Tanaka, C. Vega, L. Xu, L.G.M. Pettersson, Water: a tale of two liquids, Chem. Rev. 116 (2016) 7463–7500, https://doi.org/10.1021/acs.chemrev.5b00750
[5] P.H. Poole, F. Sciortino, U. Essmann, H.E. Stanley, Phase behaviour of metastable water, Nature 360 (1992) 324–328, https://doi.org/10.1038/360324a0
[6] P.G. Debenedetti, F. Sciortino, G.H. Zerze, Second critical point in two realistic models of water, Science 369 (2020) 289–292, https://doi.org/10.1126/science.abb9796
[7] K.H. Kim, K. Amann-Winkel, N. Giovambattista, A. Späh, F. Perakis, H. Pathak, M.L. Parada, C. Yang, D. Mariedahl, T. Eklund, T.J. Lane, S. You, S. Jeong, M. Weston, J.H. Lee, I. Eom, M. Kim, J. Park, S.H. Chun, P.H. Poole, A. Nilsson, Experimental observation of the liquid-liquid transition in bulk supercooled water under pressure, Science 370 (2020) 978–982, https://doi.org/10.1126/science.abb9385
[8] R. Foffi, F. Sciortino, Identification of local structures in water from supercooled to ambient conditions, J. Chem. Phys. 160 (2024) 094504, https://doi.org/10.1063/5.0188764

[9] Y. Guo, F.E. Maturi, C.D.S. Brites, L.D. Carlos, Exploring green fluorescent protein brownian motion: temperature and concentration dependencies through luminescence thermometry, Adv. Phys. Res. 3 (2024) 2400085, https://doi.org/10.1002/apxr.202400085

[10] F.E. Maturi, R.S. Raposo Filho, C.D.S. Brites, J. Fan, R. He, B. Zhuang, X. Liu, L.D. Carlos, Deciphering density fluctuations in the hydration water of brownian nanoparticles via upconversion thermometry, J. Phys. Chem. Lett. 15 (2024) 2606–2615, https://doi.org/10.1021/acs.jpclett.4c00044

[11] C.D.S. Brites, B. Zhuang, M.L. Debasu, D. Ding, X. Qin, F.E. Maturi, W.W.Y. Lim, D.W. Soh, J. Rocha, Z. Yi, X. Liu, L.D. Carlos, Decoding a percolation phase transition of water at ~ 330 K with a nanoparticle ruler, J. Phys. Chem. Lett. 11 (2020) 6704–6711, https://doi.org/10.1021/acs.jpclett.0c02147

[12] Y. Maréchal, The molecular structure of liquid water delivered by absorption spectroscopy in the whole IR region completed with Thermodynamics data, J. Mol. Struct. 1004 (2011) 146–155, https://doi.org/10.1016/j.molstruc.2011.07.054

[13] P.M.C. de Oliveira, J.I.R. de Souza, J.A.B. da Silva, R.L. Longo, Temperature dependence of hydrogen bond networks of liquid water: thermodynamic properties and structural heterogeneity from topological descriptors, J. Phys. Chem. B 127 (2023) 2250–2257, https://doi.org/10.1021/acs.jpcb.2c08873

[14] A. Neophytou, D. Chakrabarti, F. Sciortino, Topological nature of the liquid–liquid phase transition in tetrahedral liquids, Nat. Phys. 18 (2022) 1248–1253, https://doi.org/10.1038/s41567-022-01698-6

[15] S. McDonald, L. Ojamäe, S.J. Singer, Graph theoretical generation and analysis of Hydrogen-Bonded structures with applications to the neutral and protonated water cube and dodecahedral clusters, J. Phys. Chem. A 102 (1998) 2824–2832, https://doi.org/10.1021/jp9803539

[16] J.-L. Kuo, J.V. Coe, S.J. Singer, Y.B. Band, L. Ojamäe, On the use of graph invariants for efficiently generating hydrogen bond topologies and predicting physical properties of water clusters and ice, J. Chem. Phys. 114 (2001) 2527–2540, https://doi.org/10.1063/1.1336804

[17] G. Camisasca, D. Schlesinger, I. Zhovtobriukh, G. Pitsevich, L.G.M. Pettersson, A proposal for the structure of high- and low-density fluctuations in liquid water, J. Chem. Phys. 151 (2019) 034508, https://doi.org/10.1063/1.5100875

[18] N. Yang, C.H. Duong, P.J. Kelleher, M.A. Johnson, Capturing intrinsic site-dependent spectral signatures and lifetimes of isolated OH oscillators in extended water networks, Nat. Chem. 12 (2020) 159–164, https://doi.org/10.1038/s41557-019-0376-9

[19] L. Gunkel, A.A. Ehrhard, C.S. Krevert, B.A. Marekha, M. Bonn, M. Grechko, J. Hunger, Dynamic anti-correlations of water hydrogen bonds, Nat. Commun. 15 (2024) 10453, https://doi.org/10.1038/s41467-024-54804-y

[20] R.T. Moura Jr., A.N.C. Neto, O.L. Malta, R.L. Longo, Overlap properties of chemical bonds in generic systems including unusual bonding situations, J. Mol. Model. 26 (2020) 301, https://doi.org/10.1007/s00894-020-04535-w

[21] C.V. Santos, S.A. Monteiro, A.S.C. Soares, I.C.A. Souto, R.T. Moura Jr., Decoding chemical bonds: assessment of the basis set effect on overlap electron density descriptors and topological properties in comparison to QTAIM, J. Phys. Chem. A 127 (2023) 7997–8014, https://doi.org/10.1021/acs.jpca.3c04504

[22] C.V. Santos-Jr, E. Kraka, R.T. Moura Jr, Chemical bond overlap descriptors from multiconfiguration wavefunctions, J. Comput. Chem. 46 (2025) e27534, https://doi.org/10.1002/jcc.27534

[23] R.F.W. Bader, Atoms in Molecules: A Quantum Theory, Oxford University Press, Oxford, 1990.

[24] P.L. Popelier, Atoms in Molecules: an Introduction, Prentice Hall, Essex, 2000.

[25] F. Weinhold, C. Landis, E.G. Glendening, What is NBO analysis and how is it useful? Int. Rev. Phys. Chem. 35 (2016) 399–440, https://doi.org/10.1080/0144235X.2016.1192262

[26] F. WEINHOLD, C.R. LANDIS, Natural bond orbitals and extensions of localized bonding concepts, Chem. Educ. Res. Pract. 2 (2001) 91–104, https://doi.org/10.1039/B1RP90011K

[27] A. Likas, N. Vlassis, J.J. Verbeek, The global k-means clustering algorithm, Pattern Recognit. 36 (2003) 451–461, https://doi.org/10.1016/S0031-3203(02)00060-2

[28] D. Steinley, K-means clustering: a half-century synthesis, Br. J. Math. Stat. Psychol. 59 (2006) 1–34, https://doi.org/10.1348/000711005X48266

[29] A. Rognoni, R. Conte, M. Ceotto, How many water molecules are needed to solvate one? Chem. Sci. 12 (2021) 2060–2064, https://doi.org/10.1039/D0SC05785A

[30] F.N. Pansini, A.J. Varandas, On the solvation model and infrared spectroscopy of liquid water, Chem. Phys. Lett. 801 (2022) 139739, https://doi.org/10.1016/j.cplett.2022.139739

[31] L. Pauling, The Nature of the Chemical Bond and the Structure of Molecules and Crystals: an Introduction to Modern Structural Chemistry, third ed, vol. 12, Cornell University Press, 1960, p. 473.

[32] M.J. Frisch, G.W. Trucks, H.B. Schlegel, G.E. Scuseria, M.A. Robb, J.R. Cheeseman, G. Scalmani, V. Barone, G.A. Petersson, H. Nakatsuji, et al., Gaussian 16 Revision C.01, Gaussian Inc, Wallingford CT, 2016.

[33] R.G. Parr, W. Yang, Density-Functional Theory of Atoms and Molecules, Oxford University Press, New York, 1989.

[34] J.-D. Chai, M. Head-Gordon, Long-range corrected hybrid density functionals with damped atom–atom dispersion corrections, Phys. Chem. Chem. Phys. 10 (2008) 6615–6620, https://doi.org/10.1039/B810189B

[35] J. Tomasi, B. Mennucci, R. Cammi, Quantum mechanical continuum solvation models, Chem. Rev. 105 (2005) 2999–3094, https://doi.org/10.1021/cr9904009

[36] D. Moscato, G. Mandelli, M. Bondanza, F. Lipparini, R. Conte, B. Mennucci, M. Ceotto, Unraveling water solvation effects with quantum mechanics/molecular mechanics semiclassical vibrational spectroscopy: the case of thymidine, J. Am. Chem. Soc. 146 (2024) 8179–8188, https://doi.org/10.1021/jacs.3c12700

[37] R. Krishnan, J.S. Binkley, R. Seeger, J.A. Pople, Self-consistent molecular orbital methods. XX. A basis set for correlated wave functions, J. Chem. Phys. 72 (1980) 650–654, https://doi.org/10.1063/1.438955

[38] E.C. Meng, T.D. Goddard, E.F. Pettersen, G.S. Couch, Z.J. Pearson, J.H. Morris, T.E. Ferrin, UCSF ChimeraX: tools for structure building and analysis, Protein Sci. 32 (2023) e4792, https://doi.org/10.1002/pro.4792

[39] M.L. Waskom, Seaborn: statistical data visualization, J. Open Source Softw. 6 (2021) 3021, https://doi.org/10.21105/joss.03021

[40] J. Wilson, E. Bright, Some mathematical methods for the study of molecular vibrations, J. Chem. Phys. 9 (1941) 76–84, https://doi.org/10.1063/1.1750829

[41] E. Kraka, M. Quintano, H.W. LaForce, J.J. Antonio, M. Freindorf, The local vibrational mode theory and its place in the vibrational spectroscopy arena, J. Phys. Chem. A 126 (2022) 8781–8798, https://doi.org/10.1021/acs.jpca.2c05962

[42] E. Kraka, W. Zou, Y. Tao, Decoding chemical information from vibrational spectroscopy data: local vibrational mode theory, WIREs comput, Mol. Sci. 10 (2020) 1480, https://doi.org/10.1002/wcms.1480

[43] Z. Konkoli, D. Cremer, A new way of analyzing vibrational spectra. I. Derivation of adiabatic internal modes, Int. J. Quantum Chem. 67 (1998) 1–9, https://doi.org/10.1002/(SICI)1097-461X(1998)67:1<1::AID-QUA1>3.0.CO;2-Z

[44] M. Quintano, R.T. Moura Jr., E. Kraka, Local vibrational mode theory meets graph theory: complete and non–redundant local mode sets, Chem. Phys. Lett. 849 (2024) 141416–1–1141416–13, https://doi.org/10.1016/j.cplett.2024.141416

[45] R.T. Moura Jr., M. Quintano, C.V. Santos-Jr, V.A. Albuquerque, E.C. Aguiar, E. Kraka, A.N. CarneiroNeto, Featuring a new computational protocol for the estimation of intensity and overall quantum yield in lanthanide chelates with applications to EU(III) mercapto-triazole schiff base ligands, Opt. Mater.: X 16 (2022) 100216–1–100216–15, https://doi.org/10.1016/j.omx.2022.100216

[46] M. Quintano, A.A.A. Delgado, R.T. Moura Jr, M. Freindorf, E. Kraka, Local mode analysis of characteristic vibrational coupling in nucleobases and watson–crick base pairs of DNA, electron, Struct. 4 (12) (2022) 044005–1– 044005–17. https://doi.org/10.1088/2516-1075/acaa7a

[47] A. Madushanka, R.T. Moura, Jr., N. Verma, E. Kraka, Quantum mechanical assessment of protein–ligand hydrogen bond strength patterns: insights from semiempirical Tight-Binding and local vibrational mode theory, Int. J. Mol. Sci. 24 (2023) 6311–1–6311–24, https://doi.org/10.3390/ijms24076311

[48] M. Quintano, R.T. Moura, Jr., E. Kraka, The pk_a rule in light of local mode force constants, Chem. Phys. Lett. 826 (2023) 140654–1–140654–7, https://doi.org/10.1016/j.cplett.2023.140654

[49] J.J. Antonio, E. Kraka, Non-covalent π–interactions in mutated aquomet-myoglobin proteins: a QM/MM and local vibrational mode study, Biochemistry 62 (2023) 2325–2337, https://doi.org/10.1021/acs.biochem.3c00192

[50] M. Freindorf, J. Antonio, E. Kraka, Hydrogen sulfide ligation in hemoglobin I of *Lucina pectinata* – a QM/MM and local mode study, J. Phys. Chem. A 127 (2023) 8316–8329, https://doi.org/10.1021/acs.jpca.3c04399

[51] F. Bodo, A. Erba, E. Kraka, R.T. Moura Jr., Chemical bonding in uranium-based materials: a local vibrational mode case study of $CS_2UO_2CL_4$ and UCl_4 crystals, J. Comput. Chem. 45 (2024) 1130–1142, https://doi.org/10.1002/jcc.27311

[52] M. Quintano, R.T. Moura, Jr., E. Kraka, Exploring Jahn-Teller distortions: a local vibrational mode perspective, J. Mol. Model. 30 (2024) 102–1–102–12, https://doi.org/10.1007/s00894-024-05882-8

[53] A. Madushanka, R.T. Moura, Jr., E. Kraka, QM40, realistic quantum mechanical dataset for machine learning in molecular science, Sci. Data 11 (2024) 1376–1–1376–6. https://doi.org/10.1038/s41597-024-04206-y

[54] F.C. Machado, M. Quintano, C.V. Santos Jr., A.N.C. Neto, E. Kraka, R.L. Longo, R.T. Moura Jr., Theoretical insights into the vibrational spectra and chemical bonding of LN(III) complexes with a tripodal N_4O_3 ligand along the lanthanide series, Phys. Chem. Chem. Phys. 27 (2025) 1794–1803, https://doi.org/10.1039/d4cp03677h

[55] L.F. Saraiva, A.N. Carneiro Neto, A.G. Bispo-Jr., M.M. Quintano, E. Kraka, L.D. Carlos, S.A.M. Lima, A.M. Pires, R.T. Moura Jr., Role of vibronic coupling for the dynamics of intersystem crossing in Eu3+ complexes: an avenue for brighter compounds, J. Chem. Theory Comput. 21 (2025) 3066–3076, https://doi.org/10.1021/acs.jctc.4c01461

[56] R. Kalescky, W. Zou, E. Kraka, D. Cremer, Local vibrational modes of the water dimer – comparison of theory and experiment, Chem. Phys. Lett. 554 (2012) 243–247, https://doi.org/10.1016/j.cplett.2012.10.047

[57] A.A.A. Delgado, D. Sethio, I. Munar, V. Aviyente, E. Kraka, Local vibrational mode analysis of ion–solvent and solvent–solvent interactions for hydrated Ca^{2+}, Clust, J. Chem. Phys. 153 (2020) 224303–1–224303–11, https://doi.org/10.1063/5.0034765

[58] A.A.A. Delgado, D. Sethio, E. Kraka, Assessing the intrinsic strengths of Ion-Solvent and Solvent-Solvent interactions for hydrated Mg^{2+}, Clusters, Inorganics 9 (2021) 31–1–31–18, https://doi.org/10.3390/inorganics9050031

[59] S. Nanayakkara, Y. Tao, E. Kraka, Capturing individual hydrogen bond strengths in ICES via periodic local vibrational mode theory: beyond the lattice energy picture, J. Chem. Theory Comput. 18 (2022) 562–579, https://doi.org/10.1021/acs.jctc.1c00357

[60] R.T. Moura, Jr., M. Quintano, J.J. Antonio, M. Freindorf, E. Kraka, Automatic generation of local vibrational mode parameters: from small to large molecules and QM/MM systems, J. Phys. Chem. A 126 (2022) 9313–9331, https://doi.org/10.1021/acs.jpca.2c07871

[61] W. Zou, R. Moura Jr., C.V. Santos-Jr., M. Quintano, F. Bodo, M. Freindorf, D. Cremer, E. Kraka, LModeA2025, Computational and Theoretical Chemistry Group (CATCO), Southern Methodist University, Dallas, TX, USA, 2025.

[62] W.G. Barbosa, C.V. Santos-Jr., R.B. Andrade, J.R. Lucena Jr, R.T. Moura Jr., Bond analysis in meta- and para-substituted thiophenols: overlap descriptors, local mode

analysis, and QTAIM, J. Mol. Model. 30 (2024) 139, https://doi.org/10.1007/s00894-024-05932-1
[63] C.V. Santos-Jr., E.M. Lima, R.T. Moura Jr., Numerical integration of overlap electron densities: parallelization strategies for a good load balancing using OpenMP, Comput. Theor. Chem. 1206 (2021) 113457, https://doi.org/10.1016/j.comptc.2021.113457
[64] D. Cremer, E. Kraka, Chemical bonds without bonding electron density? Does the difference Electron-Density analysis suffice for a description of the chemical bond? Angew. Chem. Int. Ed. 23 (1984) 627–628, https://doi.org/10.1002/anie.198406271
[65] D. Cremer, E. Kraka, A description of the chemical bond in terms of local properties of electron density and energy, Croat. Chem. Acta 57 (1984) 1259–1281, https://hrcak.srce.hr/194019.
[66] T.A. Keith, AIMAll version 19.10.12, Todd A. Keith, TK Gristmill Software, Overland Park KS, USA, (aim.tkgristmill.com) (2019.
[67] I.V. Alabugin, M. Manoharan, S. Peabody, F. Weinhold, Electronic basis of improper hydrogen bonding: a subtle balance of hyperconjugation and rehybridization, J. Am. Chem. Soc. 125 (2003) 5973–5987, https://doi.org/10.1021/ja034656e
[68] F. Weinhold, C.R. Landis, Valency and Bonding: A Natural Bond Orbital Donor-Acceptor Perspective, Cambridge University Press, Theoretical Chemistry Institute, University of Wisconsin, Madison, Cambridge, U.K, 2003.
[69] C. Shi, B. Wei, S. Wei, W. Wang, H. Liu, J. Liu, A quantitative discriminant method of elbow point for the optimal number of clusters in clustering algorithm, J. Wirel. Com. Netw. 2021 (2020), https://doi.org/10.1186/s13638-021-01910-w
[70] N.T. Sagala, A.A. Gunawan, Discovering the optimal number of crime cluster using elbow, silhouette, gap statistics, and NbClust methods, ComTech: computer, Math. Eng. Appl. (2022), https://doi.org/10.21512/comtech.v13i1.7270
[71] A. Punhani, N. Faujdar, K. Mishra, D.M. SUBRAMANIAN, Binning-Based silhouette approach to find the optimal cluster using K-Means, IEEE Access 10 (2022) 115025–115032, https://doi.org/10.1109/ACCESS.2022.3215568
[72] P. Wernet, D. Nordlund, U. Bergmann, M. Cavalleri, M. Odelius, H. Ogasawara, L.Å. Näslund, T.K. Hirsch, L. Ojamäe, P. Glatzel, L.G.M. Pettersson, A. Nilsson, The structure of the first coordination shell in liquid water, Science 304 (2004) 995–999, https://doi.org/10.1126/science.1096205
[73] J. Stenger, D. Madsen, P. Hamm, E.T.J. Nibbering, T. Elsaesser, Ultrafast vibrational dephasing of liquid water, Phys. Rev. Lett. 87 (2001) 027401, https://doi.org/10.1103/PhysRevLett.87.027401
[74] K.P. Sinaga, M.-S. Yang, Unsupervised k-means clustering algorithm, IEEE Access 8 (2020) 80716–80727, https://doi.org/10.1109/ACCESS.2020.2988796
[75] E. Kraka, J.A. Larsson, D. Cremer, Generalization of the badger rule based on the use of adiabatic vibrational modes, In J. Grunenberg (Ed.), Computational Spectroscopy, Wiley, New York, 2010, pp. 105–149, https://doi.org/10.1002/9783527633272.ch4
[76] M. Freindorf, E. Kraka, D. Cremer, A comprehensive analysis of hydrogen bond interactions based on local vibrational modes, Int. J. Quantum Chem. 112 (2012) 3174–3187, https://doi.org/10.1002/qua.24118
[77] H. Humaira, R. Rasyidah, Determining the appropiate cluster number using elbow method for K-Means algorithm, in: Proceedings of the Proceedings of the 2nd Workshop on Multidisciplinary and Applications (WMA) 2018, 24-25 January 2018, Padang, Indonesia, 2020, https://doi.org/10.4108/eai.24-1-2018.2292388
[78] S.A.P. Raj, V. Thulasiraman, Determining optimal number of k for e-learning groups clustered using k-medoid, Int. J. Adv. Comput. Sci. Appl. 12 (2021), https://doi.org/10.14569/IJACSA.2021.0120644
[79] A.K. Soper, M.A. Ricci, Structures of High-Density and Low-Density water, Phys. Rev. Lett. 84 (2000) 2881, https://doi.org/10.1103/PhysRevLett.84.2881
[80] R. Foffi, J. Russo, F. Sciortino, Structural and topological changes across the liquid–liquid transition in water, J. Chem. Phys. 154 (2021) 184506, https://doi.org/10.1063/5.0049299
[81] M. Förster, N. Ukoji, C.J. Sahle, J. Niskanen, R. Sakrowski, G. Surmeier, C. Weis, T. Irifune, S. Imoto, H. Yavas, et al., Generating interstitial water within the persisting tetrahedral H-bond network explains density increase upon compressing liquid water, proc, Proc. Natl. Acad. Sci. U.S.A. 121 (2024) e2403662121, https://doi.org/10.1073/pnas.2403662121
[82] S. Fanetti, A. Lapini, M. Pagliai, M. Citroni, M. Di Donato, S. Scandolo, R. Righini, R. Bini, Structure and dynamics of Low-Density and High-Density liquid water at high pressure, J. Phys. Chem. Lett. 5 (2014) 235–240, https://doi.org/10.1021/jz402302z
[83] A. Priyadarshini, A. Biswas, D. Chakraborty, B.S. Mallik, Structural and thermophysical anomalies of liquid water: a tale of molecules in the instantaneous low- and High-Density regions, J. Phys. Chem. B 124 (2020) 1071–1081, https://doi.org/10.1021/acs.jpcb.9b11596
[84] M. Li, L. Chen, L. Gui, S. Cao, D. Liu, G. Zhao, M. Ding, J. Yan, D. Wang, Born–oppenheimer molecular dynamics simulations on structures of high-density and low-density water: a comparison of the SCAN meta-GGA and PBE GGA functionals, Phys. Chem. Chem. Phys. 23 (2021) 2298–2304, https://doi.org/10.1039/D0CP05707J